Variability in the Characteristics of Precipitation Systems in the Tropical Pacific. Part II: Implications for Atmospheric Heating

TRISTAN S. L'ECUYER, HIROHIKO MASUNAGA, AND CHRISTIAN D. KUMMEROW

Colorado State University, Fort Collins, Colorado

ABSTRACT

This paper explores changes in the principal components of observed energy budgets across the tropical Pacific in response to the strong 1998 El Niño event. Multisensor observations from the Tropical Rainfall Measuring Mission (TRMM) Microwave Imager (TMI), Visible and Infrared Scanner (VIRS), and precipitation radar (PR) instruments aboard TRMM are used to quantify changes in radiative and latent heating in the east and west Pacific in response to the different phases of the El Niño–Southern Oscillation. In periods of normal east–west SST gradients there is substantial heating in the west Pacific and cooling in the east, implying strong eastward atmospheric energy transport. During the active phase of the El Niño, both the east and west Pacific tend toward local radiative–convective equilibrium resulting in their temporary energetic decoupling. It is further demonstrated that the response of these regions to ENSO-induced SST variability is directly related to changes in the characteristics of clouds and precipitation in each region. Through quantitative analysis of the radiative and latent heating properties of shallow, midlevel, and deep precipitation events and an equivalent set of nonprecipitating cloud systems, times of reduced atmospheric heating are found to be associated with a shift toward shallow and midlevel precipitation systems and associated low-level cloudiness. The precipitation from such systems is typically less intense, and they do not trap outgoing longwave radiation as efficiently as their deeper counterparts, resulting in reduced radiative and latent heating of the atmosphere. The results also suggest that the net effect of precipitating systems on top-of-the-atmosphere (TOA) fluxes and the efficiency with which they heat the atmosphere and cool the surface exhibit strong dependence on their surroundings. The sensitivity of cloud radiative impacts to the atmospheric and surface properties they act to modify implies the existence of strong feedbacks whose representation may pose a significant challenge to the climate modeling community.

1. Introduction

Globally, atmospheric radiative cooling through the emission of thermal radiation to space and the surface is balanced by the absorption of solar radiation and the transfer of energy from the surface to the atmosphere in the form of latent and sensible heating. This radiative–convective equilibrium (RCE), however, seldom occurs locally because of the highly variable nature of the frequency, structure, and radiative properties of clouds and precipitation. This variability leads to substantial regional imbalances in atmospheric heating that drive large-scale circulation patterns. Numerous studies have sought to characterize the impacts of cloud radia-

tive heating and latent heating from precipitation on scales ranging from those of individual mesoscale convective systems (e.g., Houze 1982, 1989; Mapes and Houze 1995), intraseasonal oscillations (e.g., Lau and Peng 1987; Lee et al. 2001), and the strength of the Hadley circulation (e.g., Slingo and Slingo 1988, 1991) and Walker circulation (e.g., Hartmann et al. 1984; Sherwood et al. 1994). The common conclusion to be drawn from these studies is the importance of accurately representing the processes that govern the microphysical properties of clouds and precipitation in order to reliably model their impact on atmospheric radiative heating.

A key obstacle to properly modeling the influence of clouds in climate is the problem of understanding and ultimately representing critical feedback processes that occur as a result of the strong interdependence between radiation, clouds, precipitation, and the environments in which they reside (Stephens 2005). It has been con-

Corresponding author address: Dr. Tristan L'Ecuyer, Department of Atmospheric Science, Colorado State University, Fort Collins, CO 80549.
E-mail: tristan@atmos.colostate.edu

jectured, for example, that increases in highly reflective cirrus clouds in response to increasing sea surface temperature (SSTs) act to limit temperatures in the ocean mixed layer to less than 305 K (Ramanathan and Collins 1991). Alternatively, Lindzen et al. (2001) propose that clouds act as an iris, opening and closing to regulate the amount of longwave (LW) radiation emitted to space in response to increases or decreases in SST. They conjecture that the area of moist cloudy regions decreases with increasing SST in such a way that their ability to trap longwave radiation decreases more rapidly than their ability to reflect solar radiation, thereby modulating SSTs. Both studies employ simple models to quantify the impacts of the proposed feedbacks that invariably invoke a number of assumptions that significantly influence interpretation of their results. Consequently, these studies have been attacked on the basis of the appropriateness of these assumptions such as the magnitude of assumed atmospheric heat transports or prescribed cloud optical properties (Pierrehumbert 1995; Lin et al. 2002; Chambers et al. 2002; Hartmann and Michelsen 2002). The recent study by Rapp et al. (2005), for example, found no systematic variation in convective cloud area normalized by precipitation with increasing SST.

Recent studies using both (relatively) simple models (e.g., Bretherton and Sobel 2002; Sobel and Gildor 2003) and more complex general circulation models (GCMs) (e.g., Lee et al. 2001) have also demonstrated the sensitivity of models to parameterizations of the radiative impacts of clouds associated with convection. The strength of the modeled Walker circulation, the propagation speed of tropical intraseasonal oscillations, and the ability of clouds to suppress hot spots in these examples are all highly sensitive to the modeled strength of cloud–radiation feedbacks regardless of specific details that govern how they impact the model.

Despite the implications of these studies, progress toward understanding cloud feedback processes in the atmosphere has been slow, as evidenced by the fact that the Intergovernmental Panel on Climate Change (IPCC) has concluded that they represent a primary source of uncertainty in predicting the impacts of climate change in each of their last three assessments. Given the variability in the magnitude of cloud heating in current GCMs owing to, for example, their sensitivity to fall speed parameterization (Jakob 2002), the challenge of quantifying relationships between the energetic properties of precipitation systems and the processes by which they form falls to the observational community. Numerous studies have been conducted over the past three decades focusing on determining the impact of regional variations in cloudiness on the

earth's radiation budget (e.g., Vonder Haar and Suomi 1971; Gray 1973; Hartmann and Short 1980; Arking 1991; Stephens and Greenwald 1991a,b; Hartmann et al. 1992; Del Genio and Kovari 2002, to name but a few). Building on the results of these works, this study and a companion paper by Masunaga et al. (2005, hereafter, Part I) make use of recent data from the Tropical Rainfall Measuring Mission satellite (TRMM) to explore the changes in the character of clouds and precipitation in response to SST variability in the Pacific Ocean. Unlike many previous studies, however, we further explore the manner by which these changes in turn impact the energetic properties of their surroundings. Our primary focus is to quantify the coupled response of clouds, precipitation, and atmospheric energetics in three regions in the tropical Pacific to the different phases of the El Niño–Southern Oscillation (ENSO). Rather than seeking to discover a grand cloud feedback mechanism like those proposed by Ramanathan and Collins (1991) or Lindzen et al. (2001), however, our goal is to provide insights into the important processes that warrant further study in order to accurately represent them in a complete theory of global climate change.

The results indicate that the radiative heating from precipitating cloud systems varies systematically with SST, precipitable water (W, and surface wind speed anomalies associated with the strong 1998 El Niño event. By virtue of changes in the relative frequencies of occurrence of different cloud systems, the west Pacific transforms from a region of intense atmospheric heating in the presence of normal SST gradients across the Pacific to conditions of approximate local RCE during the El Niño event. Conversely, a substantial increase in the occurrence of deep convection modifies the east Pacific, normally a region of strong radiative cooling, into a heating region. As a result, the implied eastward transport of energy is temporarily halted in agreement with the observed reduced strength of the Walker circulation. While the influence of ENSO on the strength of the Walker circulation has been known for some time, the analysis establishes the connection between variations in atmospheric heating in the Pacific to changes in the relative frequency of occurrence of different precipitating cloud systems in response to ENSO-induced SST variability.

Unlike many prior studies that are based on regional datasets or model-derived fields, the analysis conducted here makes use of an extensive set of satellite-derived products that offer spatial coverage afforded by models but avoid the need to parameterize important physical processes. The observationally based conclusions regarding relationships between radiation and hydrology

that emerge from this study therefore provide an independent test of the combined effects of the parameterizations that lie at the root of numerical weather prediction (NWP) and climate models. The results demonstrate the need for models to explicitly represent differences in the radiative properties of distinct cloud systems and support the use of observations to provide guidance concerning the response of cloud distributions to particular modes of climate variability.

Section 2 describes the algorithm and relevant datasets used to estimate radiative and latent heat fluxes from TRMM observations. The overall energy budgets of the east and west tropical Pacific are explored in section 3, and their properties under conditions characteristic of a strong El Niño event are compared to those representative of the climatological mean in the region. Section 4 quantifies the energetic properties of each storm type identified in Part I as well as a number of nonprecipitating pixel classes and decomposes the regional energy budgets into components owing to each pixel type. Finally, the implications of changes in the regionally averaged radiative heating and cooling efficiencies of precipitating systems for modeling the impacts of clouds in global climate change will be addressed in section 5.

2. Analysis approach

The analysis that follows derives from a combination of the storm type classification methodology outlined in Part I and the technique for estimating components of the atmospheric energy budget and hydrologic cycle from satellite observations developed in L'Ecuyer and Stephens (2003, hereafter LS03). The salient features of these techniques will be described here, but the interested reader is encouraged to read those manuscripts for further details.

a. Pixel classification

Traditional approaches to classifying clouds and rainfall systems have focused on either measurements of infrared brightness temperature (T_B) that are representative of cloud-top height or vertical structure information obtained from radar observations that is typically most sensitive to precipitation. Part I demonstrated the utility of combining these observations to develop a classification that simultaneously captures properties of the precipitation and associated cloud fields to provide a more complete representation of the microphysical properties of the precipitation system as a whole. In this study, we follow the procedure outlined in Part I to classify precipitation systems based on their 10.8-μm T_B

TABLE 1. Definition of storm categories. Adapted from Part I.

Storm category	Radar echo-top height	Infrared T_B
Shallow	<4 km	>260 K
Cumulus congestus	4–6 km	>245 K
Deep stratiform	4–6 km	<245 K
Deep convective	>6 km	<245 K

measured by the Visible and Infrared Scanner (VIRS) and their echo-top height characterized by the precipitation radar (PR) both of which fly aboard TRMM. Histograms of these parameters created by carefully matching VIRS and PR observations suggest that most of the precipitating cloud systems observed by TRMM can be grouped into the four precipitation classes summarized in Table 1. Storms with echo tops less than 4 km and T_Bs warmer than 260 K are appropriately classified as "shallow" precipitation. At the other end of the spectrum, "deep convective" precipitation events are defined as those having cloud tops colder than 245 K and echo tops in excess of 6 km. Between these extremes two additional storm categories are defined both with echo tops near the freezing level between 4 and 6 km. The "deep stratiform" category exhibits cloud tops colder than 245 K while the "cumulus congestus" category has cloud tops warmer than this threshold. Some justification for the distinction between these two storm types is provided in Part I by the fact that the deep stratiform category is dominated by stratiform precipitation while the cumulus congestus category is composed primarily of convective rainfall (as defined by the TRMM PR-based 2A23 product described below).

Since the primary objective of this paper is to examine the radiative properties of the various cloud systems observed in the Tropics, it is also important to identify clouds in nonprecipitating regions so that their contribution to the energetic properties of the tropical atmosphere can also be identified. To this end, two additional components are added to the classification described above, an infrared high cloud mask again using VIRS and a low cloud mask derived from TRMM Microwave Imager (TMI) observations, both of which are described in greater detail below.

b. The Hydrologic Cycle and Earth Radiation Budget algorithm

Corresponding radiative flux and heating rate profiles are estimated following the technique outlined in LS03. The approach, known as the Hydrologic Cycle and Earth Radiation Budget (HERB) algorithm, syn-

thesizes complementary information from the sensors aboard TRMM, to initialize broadband radiative transfer calculations for deriving the spatial and temporal distribution of radiative heating in the tropical atmosphere. Distinct retrievals of high-cloud optical properties using VIRS (Cooper et al. 2003), liquid clouds from TMI (Greenwald et al. 1993), and precipitation from the TMI-based Goddard Profiling Algorithm (GPROF; Kummerow et al. 2000) are first combined to obtain a composite view of the three-dimensional structure of clouds and precipitation in the atmosphere. Surface rainfall estimates from GPROF are used to discriminate between raining and nonraining pixels. In all pixels with nonzero surface rainfall rates, liquid and ice hydrometeor profiles from GPROF are adopted, and collocated 10.8-μm radiances from VIRS are used to constrain cloud-top height. VIRS and TMI observations are then used to establish the presence and properties of liquid and ice clouds in all other pixels. Any pixel for which the VIRS 10.8-μm T_B falls more than 5 K below the climatological mean clear-sky value is considered to contain a high cloud. Low-lying liquid clouds, on the other hand, are identified using the liquid water path retrieval algorithm described by Greenwald et al. (1993). Any pixel with LWP exceeding 0.05 kg m^{-2} is considered to contain a low cloud. While neither of these masks are devoid of false detections or missed clouds, they provide adequate qualitative information to categorize the data on the time and spatial scales of interest to this study. Based on the detailed error analysis of LS03, uncertainties introduced through missed and/or false detections resulting from these procedures are expected to be ~5 and 10 W m^{-2} in longwave and shortwave (SW) fluxes, respectively.

These cloud and precipitation fields are supplemented with profiles of temperature and humidity from European Centre for Medium-Range Weather Forecasts (ECMWF) analyses, ocean surface properties from Remote Sensing Systems (RSSs), and a crude model of the global distribution of aerosol optical properties from the Global Aerosol Climatology Project (GACP). The data are subsequently mapped onto a uniform 0.25° grid to facilitate footprint matching and used as input to a broadband radiative transfer model to compute upwelling and downwelling LW and SW radiative flux profiles for each pixel. The model, known as BUGSrad, is founded on the δ-two-stream approximation to the radiative transfer equation (e.g., Stephens et al. 2001). It is applied over 6 SW and 12 LW spectral bands and accounts for the effects of scattering, absorption, and emission from all four hydrometeor classes retrieved by GPROF using the parameterization of cloud optical properties introduced in Stephens et al.

(1990). Computed flux profiles are used to derive principal components of the radiation budget and their breakdown into clear-sky and cloudy components. In the case of precipitating pixels, an estimate of column-integrated latent heating (LH) is also made using LH = $\rho_l L_v R$, where ρ_l is the density of liquid water, L_v is the latent heat of vaporization, and R is the retrieved surface rainfall rate. This relationship is only justified on spatial and temporal scales that encompass the complete life cycle of precipitating cloud systems, a good assumption for the large regions and monthly averages considered here (see LS03 for more details).

LS03 perform an extensive analysis of the uncertainties in all components of the algorithm using a combination of sensitivity studies and detailed comparisons with observed top-of-the-atmosphere (TOA) fluxes. Direct propagation of the uncertainties in all input parameters through the algorithm demonstrate that the technique provides monthly mean estimates of oceanic LW fluxes at 1° resolution to an accuracy of 10 W m^{-2}. Corresponding SW flux estimates are found to be accurate to 25 W m^{-2}. After careful examination of the sources of these errors, LS03 conclude that uncertainties in LW fluxes are dominated by the lack of ice cloud vertical placement information in the VIRS observations as well as errors in the vertical distribution of water vapor, particularly in the upper troposphere. Uncertainties in SW fluxes, on the other hand, are dominated by errors in the detection of low clouds and poorly constrained liquid cloud microphysical properties. These estimates are consistent with the comparisons of outgoing LW and SW radiative flux estimates at 1.0° resolution to observations from the Clouds and the Earth's Radiant Energy System (CERES) instrument (Wielicki et al. 1996). Root-mean-square differences in monthly means outgoing longwave radiation (OLR) and outgoing shortwave radiation (OSR) are 8 and 21 W m^{-2}, respectively, while corresponding differences in instantaneous fluxes are 30 and 77 W m^{-2}.

c. Datasets

Together, the HERB products and the classification scheme described above make it possible to probe the role of various precipitating cloud systems in defining regional energy budgets in the Tropics. This study combines four distinct TRMM products covering the months of February 1998 during the strong 1998 El Niño event and February 2000 that corresponded to weak La Niña conditions. The 1B01 VIRS calibrated radiance product supplies the 10.8-μm T_B information to constrain cloud-top height while storm echo-top height is obtained from the PR 2A23 dataset. HERB's low-cloud retrievals make use of vertically and horizon-
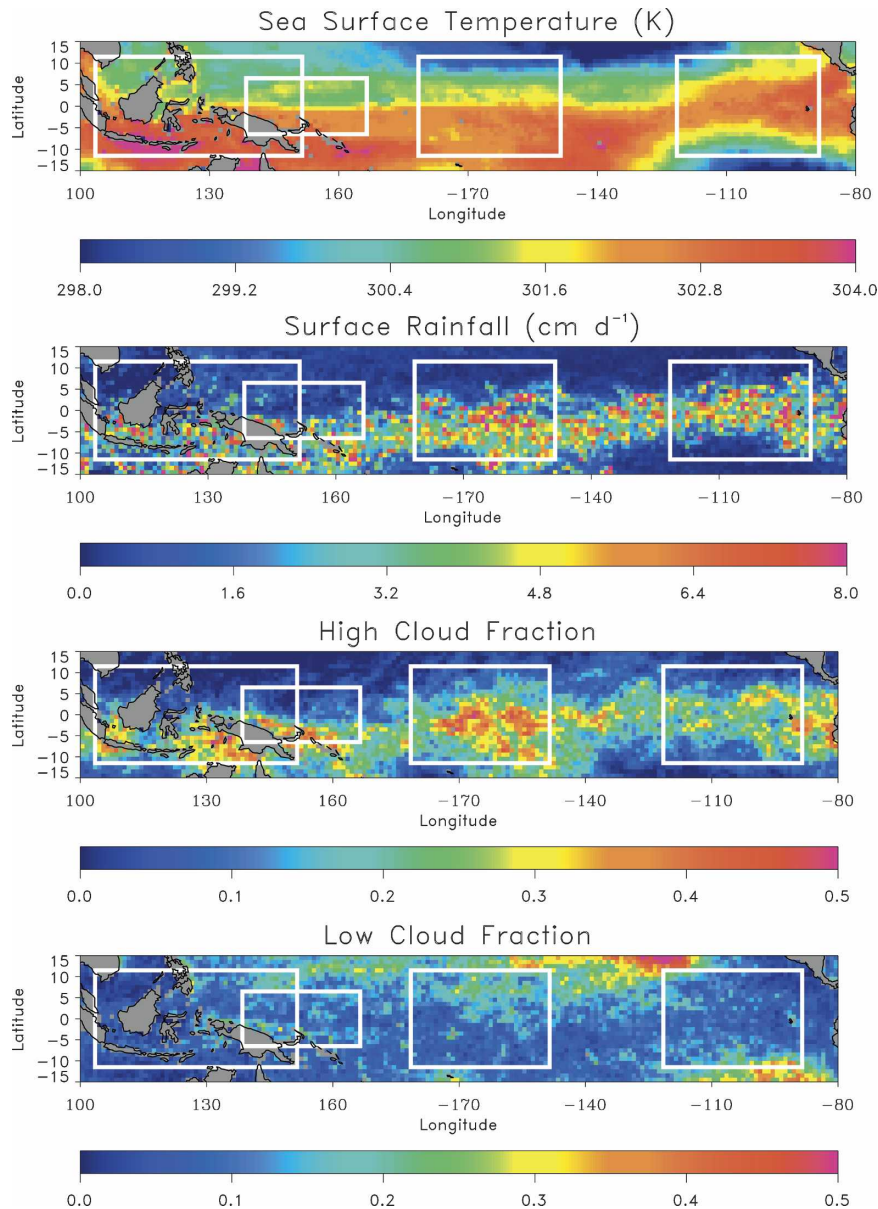
FIG. 1. Mean atmospheric and surface properties in the tropical Pacific for the month of February 1998. The TWP, TCP, and TEP regions defined for the analysis are highlighted by white rectangles. For comparison purposes, the smaller TWP region defined by Cess et al. (2001) is also highlighted.

tally polarized T_Bs from the TMI 1B11 product, and liquid and ice water content profiles for precipitating systems are obtained from the TMI-based 2A12 TMI profiling product. Detailed descriptions and access to each of these datasets is provided by the Goddard Distributed Active Archive Center (DAAC; http://lake.nascom.nasa.gov/data/dataset/TRMM/).

Three oceanic regions between 10°N and 10°S are analyzed: the tropical west Pacific (TWP: 105°–150°E), central Pacific (TCP: 180°−150°W), and east Pacific

(TEP: 120°−90°W). Selected input fields to the HERB algorithm are illustrated in Figs. 1 and 2 to highlight the differences between these regions in February 1998 and 2000. Also shown is the west Pacific region analyzed by Cess et al. (2001, hereafter CESS01) for comparison. The top panels illustrate the eastward migration of warmest SSTs during the strong El Niño event that took place in 1998 (Fig. 1) relative to more climatologically "normal" conditions in 2000 (Fig. 2). The remaining panels compare daily mean precipitation and cloud
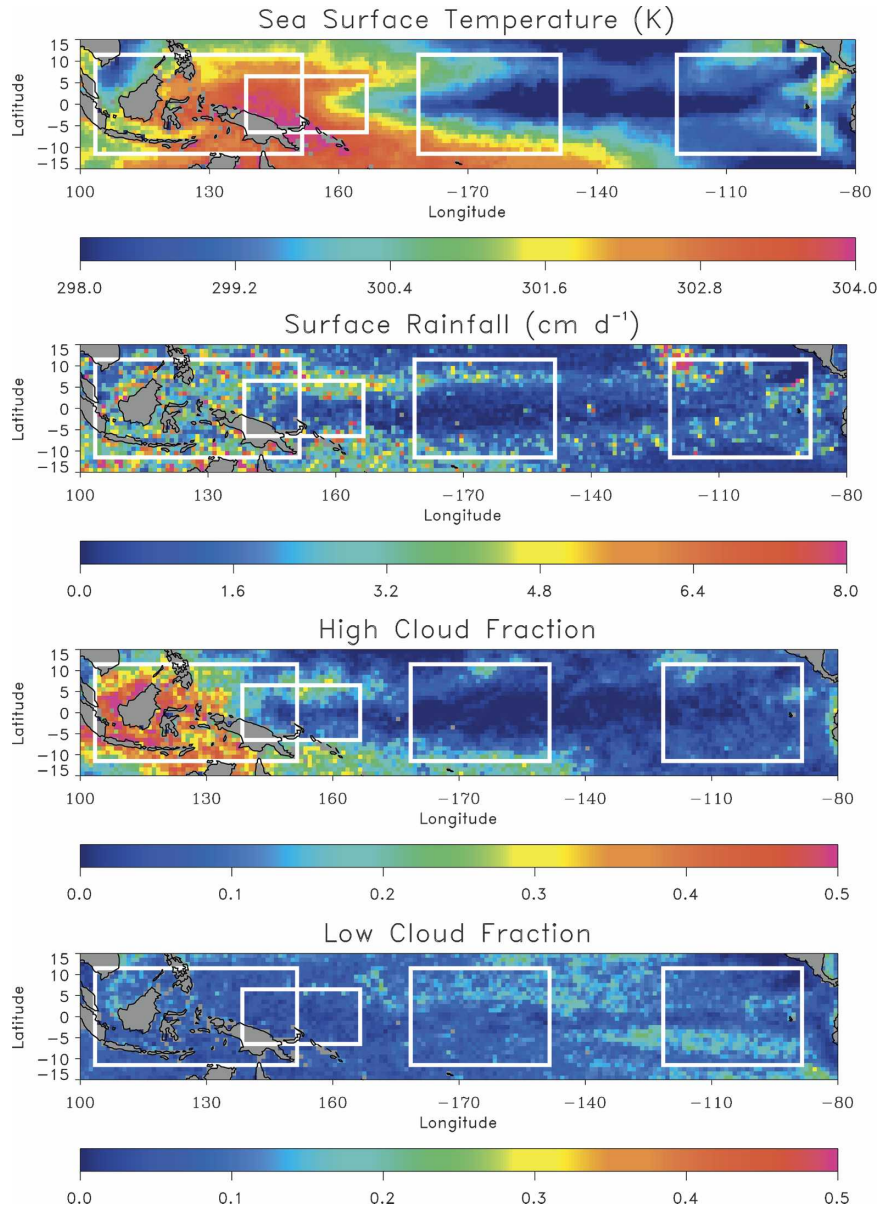
FIG. 2. Same as in Fig. 1, but for the month of February 2000.

fractions for the two months illustrating a distinct east-ward shift of intense precipitation and high clouds as-sociated with the changing SST. These figures suggest that there is a significant response in the distribution of high clouds and precipitation in response to the change in SST gradient associated with El Niño. Based on this observation, it is logical to ask how the energy balance in the east and west Pacific regions are modified by the changing character of local clouds and precipitation and, in turn, how such changes feedback on other prop-erties of the regions through changes in the circulation between them.

3. Regional energy budgets

To provide a foundation for analyzing the impacts of variations in the character of precipitating cloud sys-tems on local atmospheric energetics, it is instructive to first examine the overall energy budget in each region. Figure 3 illustrates the principal components of the at-mospheric radiation budget for the TWP in February 1998 along with corresponding error estimates based on the analysis of LS03. It is important to note that the uncertainties quoted here provide an upper bound on the uncertainties in each flux since no reduction of ran-
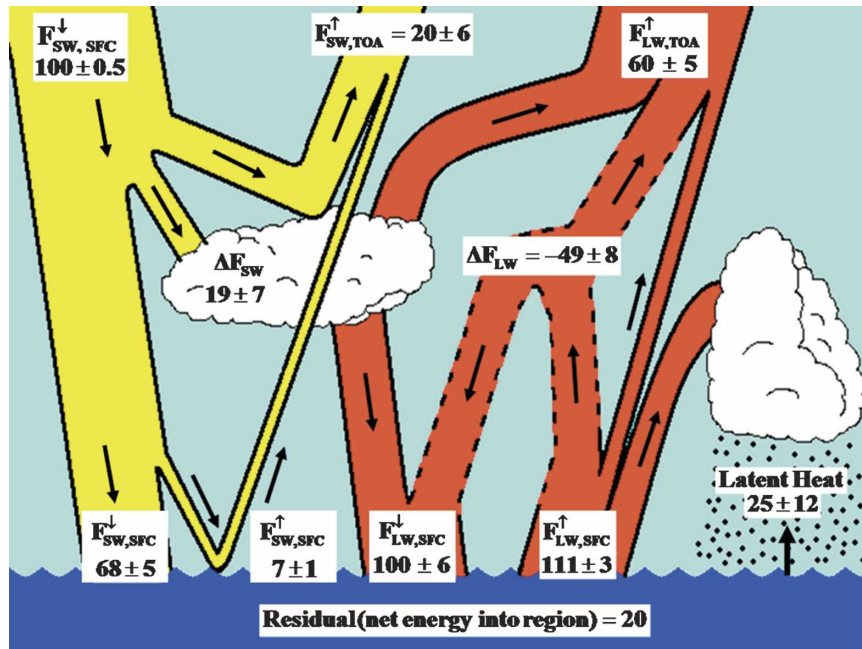
Fig. 3. Principal components of the regional energy budget of the TWP for the month of February 1998. All fluxes have been normalized by the mean solar insolation at TOA in the region for the month of February (433 W m^{-2}). The flux labels adopted here are defined in Table 1.

dom noise through temporal or spatial averaging has been accounted for. Direct comparisons with CERES TOA fluxes suggest that the estimates are likely a factor of 2 more accurate than indicated. The labels assigned to the various fluxes are defined in Table 2, where they are further decomposed into fractions owing to raining pixels, nonprecipitating cloudy pixels, and clear pixels.

The imbalance between incoming solar radiation and outgoing SW and LW fluxes results in a net surplus of radiation into the region of 95 W m^{-2}. Perhaps somewhat surprisingly, Table 2 indicates that the west Pacific, generally considered a source of atmospheric heating, is actually found to exhibit a small net cooling of $\sim$5 W m^{-2} when one compares the radiative cooling of -126 W m^{-2} to the inferred latent heat release of 28 $\times$ 4.33 = 121 W m^{-2}. This is likely accounted for by the transfer of energy from the ocean to the atmosphere in the form of sensible heat, but since this contribution is typically an order of magnitude smaller than that due to latent heating, we can conclude that the TWP very nearly exhibits local atmospheric energy balance during the 1998 El Niño event.

Equivalent results for the month of February 2000 are summarized in Table 3, for comparison. Again the region experiences a net surplus of 100 W m^{-2} of energy but now, during this period of more climatologi-

cally normal SST gradients across the Pacific, the TWP experiences a net atmospheric heating of $\sim$70 W m^{-2}. Tables 2 and 3 also indicate that the fraction of pixels containing either clouds or precipitation is significantly suppressed during the 1998 El Niño to 34% from almost 50% in the normal year. Evidence of the impact of this change can be seen in the contributions of cloudy and precipitating pixels to components of the energy budget in the region. In the normal year, for example, these pixels accounted for 67% of the solar radiation reflected to space while they accounted for only 50% in February 1998. Similarly, 41% of the outgoing longwave radiation occurs in cloudy and precipitating skies in the normal year while these conditions only account for 27% of the OLR during the 1998 El Niño.

Also summarized in Tables 2 and 3 are the cloud impacts on SW and LW fluxes at TOA defined as the difference in OSR and OLR between the all-sky conditions that are observed and an equivalent pixel with all clouds and precipitation removed. On average clouds reflect 30% more SW radiation back to space and trap almost 50% more LW radiation in the normal year consistent with the significant reduction in the frequency of occurrence of clouds and rainfall during the El Niño event. Ultimately, the reduced cloudiness and precipitation in 1998 result in increased OLR of 21 W m^{-2}, increased SW absorption of $\sim$12 W m^{-2}, and a

TABLE 2. Decomposition of the February 1998 energy budget of the TWP into three hydrologic categories: precipitating pixels (rain), nonprecipitating cloudy pixels (cloud), and clear-sky pixels (clear). The fraction of pixels that fall into each category are given in the top row. In subsequent rows, fluxes in the first column are expressed as a percentage of the mean incoming solar radiation at the TOA, 433 W m^{-2}, while remaining columns provide the percentage of the total attributed to each pixel type. The second group of rows summarize the impacts of clouds on SW and LW fluxes at TOA and SFC in W m^{-2} and their breakdown into precipitating and nonprecipitating cloud types. The last three rows summarize the net radiation budgets at the TOA, within the atmosphere, and at the surface in W m^{-2}, respectively.

Flux	Interpretation	Total	Rain	Cloud	Clear
f	Pixel fractions	100	14	20	66
$F_{SW,TOA}^{\downarrow}$	Incoming solar	100	16	18	66
$F_{SW,TOA}^{\uparrow}$	Outgoing SW	20	22	32	46
ΔF_{SW}	SW absorption	19	18	19	63
$F_{SW,SFC}^{\downarrow}$	Downwelling SW at SFC	68	13	14	73
$F_{SW,SFC}^{\uparrow}$	Upwelling SW at SFC	7	13	14	73
$F_{LW,SFC}^{\uparrow}$	Surface emission	107	14	20	66
$F_{LW,SFC}^{\downarrow}$	Downwelling LW at SFC	97	14	21	65
ΔF_{LW}	LW divergence	−48	13	14	73
$F_{LW,TOA}^{\uparrow}$	Outgoing LW	58	12	15	73
LH	Latent heat	28	100	0	0
$C_{SW,TOA}$	SW cloud impact TOA	−24	−9	−15	0
$C_{LW,TOA}$	LW cloud impact TOA	23	6	17	0
$C_{SW,SFC}$	SW cloud impact SFC	−26	−11	−15	0
$C_{LW,SFC}$	LW cloud impact SFC	5	2	3	0
F_{TOA}^{NET}	$F_{SW,TOA}^{\downarrow}-F_{SW,TOA}^{\uparrow}-F_{LW,TOA}^{\uparrow}$			94	
F_{ATM}^{NET}	$\Delta F_{SW} + \Delta F_{LW}$			−125	
F_{SFC}^{NET}	$F_{SW,SFC}^{\downarrow}+F_{LW,SFC}^{\downarrow}-F_{SW,SFC}^{\uparrow}-F_{LW,SFC}^{\uparrow}$			219	

decrease of 44 W m^{-2} in the latent heat release in the atmosphere. This is partially compensated by a small (~16 W m^{-2}) reduction in solar reflection to space, but overall the TWP atmosphere experiences both suppressed radiative and latent heating in response to the change in cloud cover associated with the 1998 El Niño.

The opposite behavior is observed in the central and

TABLE 3. Same as in Table 2, but for the month of February 2000.

Flux	Total	Rain	Cloud	Clear
f	100	21	28	51
$F_{SW,TOA}^{\downarrow}$	100	22	28	50
$F_{SW,TOA}^{\uparrow}$	24	29	38	33
ΔF_{SW}	22	25	25	50
$F_{SW,SFC}^{\downarrow}$	61	17	24	59
$F_{SW,SFC}^{\uparrow}$	6	17	24	59
$F_{LW,SFC}^{\uparrow}$	107	20	28	52
$F_{LW,SFC}^{\downarrow}$	98	21	28	51
ΔF_{LW}	−44	21	20	59
$F_{LW,TOA}^{\uparrow}$	53	20	21	59
LH	38	100	0	0
$C_{SW,TOA}$	−32	−13	−19	0
$C_{LW,TOA}$	34	10	24	0
$C_{SW,SFC}$	−29	−14	−15	0
$C_{LW,SFC}$	5	3	2	0
F_{TOA}^{NET}		101		
F_{ATM}^{NET}		−97		
F_{SFC}^{NET}		198		

east Pacific as suggested by Table 4, which summarizes the observed energy budget in the TEP region for both February 1998 and 2000. During the normal year, clouds and precipitation constitute less than 25% of the observed pixels while they make up 43% of the scenes observed in 1998. As a result, while the region as a whole experiences a net surplus of TOA radiation in both months, the atmosphere loses 67 W m^{-2} under normal SST conditions while gaining 84 W m^{-2} during the 1998 El Niño. This is a direct consequence of enhanced radiative and latent heating associated with the increased clouds and precipitation in the region in direct contrast to the El Niño response observed in the TWP.

Similar behavior is observed in the TCP (not shown) indicating that in February 2000, and presumably other periods with more or less normal SST gradients between the east and west Pacific, there is a net eastward transport of energy associated with the Walker circulation. This finding is not new, but it is reassuring that it agrees with the findings of, for example, Cornejo-Garrido and Stone (1977), who suggest that the Walker circulation is primarily driven by zonal variations in condensation. The results from February 1998 support the fact that ENSO exerts a strong influence on the strength of this circulation by significantly reducing (if not completely eliminating) the required transport of energy to establish equilibrium across the Pacific.

TABLE 4. Same as in Tables 2 and 3, but comparing the properties of the east Pacific in 1998 and 2000.

Flux	1998				2000			
	Total	Rain	Cloud	Clear	Total	Rain	Cloud	Clear
f	100	21	22	57	100	12	12	76
$F_{SW,TOA}^{\downarrow}$	100	20	20	60	100	12	11	77
$F_{SW,TOA}^{\uparrow}$	20	26	33	41	21	13	25	62
ΔF_{SW}	20	23	20	57	22	14	11	75
$F_{SW,SFC}^{\downarrow}$	67	17	15	68	65	11	6	83
$F_{SW,SFC}^{\uparrow}$	7	17	15	68	7	11	6	83
$F_{LW,SFC}^{\uparrow}$	107	21	22	57	104	12	12	76
$F_{LW,SFC}^{\downarrow}$	98	21	23	56	92	13	13	74
ΔF_{LW}	−47	20	17	63	−49	12	12	76
$F_{LW,TOA}^{\uparrow}$	56	18	17	65	61	12	11	77
LH	47	100	0	0	13	100	0	0
$C_{SW,TOA}$	−35	−14	−21	0	−16	−3	−13	0
$C_{LW,TOA}$	39	12	27	0	6	2	4	0
$C_{SW,SFC}$	−38	−16	−22	0	−16	−3	−13	0
$C_{LW,SFC}$	7	3	4	0	4	1	3	0
F_{TOA}^{NET}		104				79		
F_{ATM}^{NET}		−117				−118		
F_{SFC}^{NET}		221				197		

It is worth noting that the ratio of cloud impacts on TOA SW to LW fluxes in the TWP region during the 1998 El Niño is not as large as the value of 1.25 presented in CESS01 although it is significantly larger than that found in February 2000. The source of this discrepancy can be traced to the fact that we define the TWP region as the area bounded by 10°S–10°N, 105°–150°E while CESS01 focus on the smaller region bounded by 5°S–5°N, 140°–165°E centered farther to the east. Table 5 summarizes cloud impacts on TOA and surface LW and SW fluxes for February 1998 and 2000 over the region defined by CESS01. Over this region $N = C_{SW}/C_{LW}$ varies from 1.05 in normal conditions to 1.25 during the 1998 El Niño in excellent agreement with the differences between normal conditions and those during the 1998 El Niño reported by CESS01. From Fig. 1, there is a greater likelihood of encountering areas of low clouds in 1998 within the region defined by CESS01 while our box captures a substantial amount of convection south of 5°S, likely accounting for the observed

differences. This demonstrates an important fact that will be discussed further in the sections that follow, namely that the parameters defining the net influence of clouds on local energy balance are strong functions of the region and time period analyzed. From the modeling perspective, this suggests that one should exercise caution when employing empirically derived relationships from regional field experiments to derive parameterizations of key physical processes in the atmosphere such as the relationship between cloud LW heating and latent heating.

4. The role of different cloud systems

It is clear that the differences in the regional energy budgets associated with different phases of ENSO can be traced to changes in the distribution of clouds and precipitation in response to variability in the SST gradient between the west and east Pacific. However the mechanism that produces the observed differences goes beyond a simple increase or decrease in precipitation and cloudiness requiring also a fundamental change in the character of the precipitation systems as suggested in Part I. To quantify the effects of such changes, flux estimates from the HERB algorithm have been used to characterize the radiative and latent heating properties of each of the storm types defined in Part I.

a. The radiative properties of each cloud type

From the analysis of correlation scale length in Part I it emerged that, in a mean sense, each of the defined

TABLE 5. Comparison of cloud impacts on SW and LW radiative fluxes at TOA in February 1998 and 2000 for the region defined by CESS01. Corresponding quantities for the TWP region defined in the current study are summarized for reference. All fluxes are in W m^{-2}.

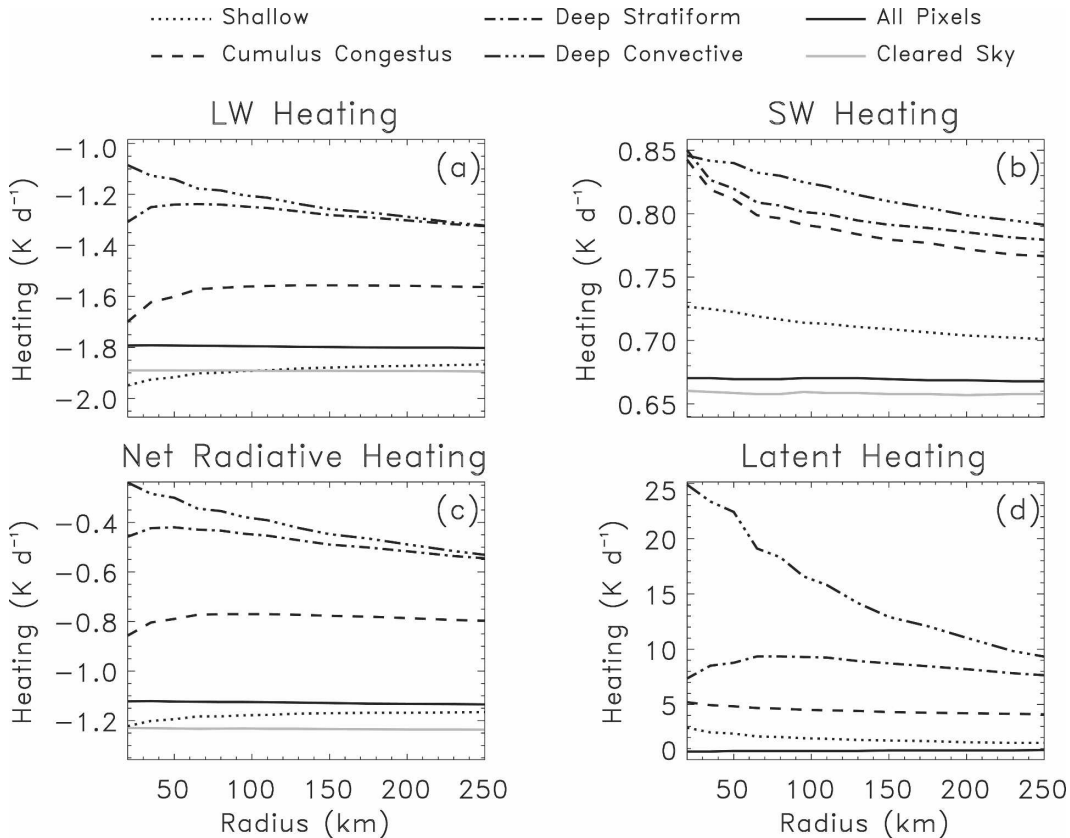| Year	Region	$C_{SW,TOA}$	$C_{LW,TOA}$	N
1998	Cess et al. TWP	−17	14	1.24
2000	Cess et al. TWP	−14	13	1.05
1998	Current study TWP	−24	23	1.05
2000	Current study TWP	−32	34	0.94

FIG. 4. Column-integrated atmospheric (a) LW radiative cooling, (b) SW radiative heating, (c) net radiative cooling, and (d) latent heating as a function of radial distance from a pixel of the type designated by the legend at the top.

storm types exhibits a unique spatial extent in terms of both rainfall and associated cloudiness. Since systems with larger horizontal scales can be expected to exhibit larger radii of influence on local energy balance, it is anticipated that different storm types will have significantly different impacts on their environment. Figure 4 compares column-integrated LW, SW, and net atmospheric radiative heating as well as atmospheric latent heating for each of the four storm categories defined in Table 1. Also shown is the mean value of these parameters for all data points within concentric circles around each type of pixel with radii ranging from 25 to 250 km calculated in a manner loosely based on the analysis of correlation scale lengths defined in Part I. The expected value of the mean value of a parameter X within a distance d_i of the reference pixel x_{ref} follows from Eq. (8) in Part I:

$$\langle X \rangle = \frac{1}{A_r} \int_{A_r} \overline{X}(d, x_{\mathrm{ref}}) \, dx_{\mathrm{ref}} \approx \frac{1}{N_{\mathrm{ref}}} \sum^{N_{\mathrm{ref}}} \overline{X}(d_i, x_{\mathrm{ref}}), \quad (1)$$

where N_{ref} is the number of pixels of the given type that fall within the area of interest, A_r, and

$$\overline{X}(d_i, x_{\mathrm{ref}}) = \frac{\sum X(d_i)}{n_{\mathrm{tot}}(d_i)} \quad (2)$$

is the mean value of X computed from the n_{tot} pixels within a distance d_i of each individual reference pixel. The sum in Eq. (1) runs over all pixels of each cloud type observed during February 1998 and 2000 and the results provide insights into the homogeneity of the environments where each type of pixel is typically found. The properties of all oceanic pixels between 25°S and 25°N (solid black curve) and an equivalent set of pixels from which all condensate has been artificially removed by ignoring clouds and precipitation in the radiative transfer calculations (solid gray curve, denoted "cleared sky") have been included for reference.

Precipitating cloud systems tend to reduce atmospheric radiative cooling by increasing the absorption of SW radiation and decreasing the emission of LW radiation. The lone exception is the shallow category, for which a slight increase in atmospheric LW cooling due to enhanced emission to the surface almost exactly balances the increase in SW heating resulting in a more-
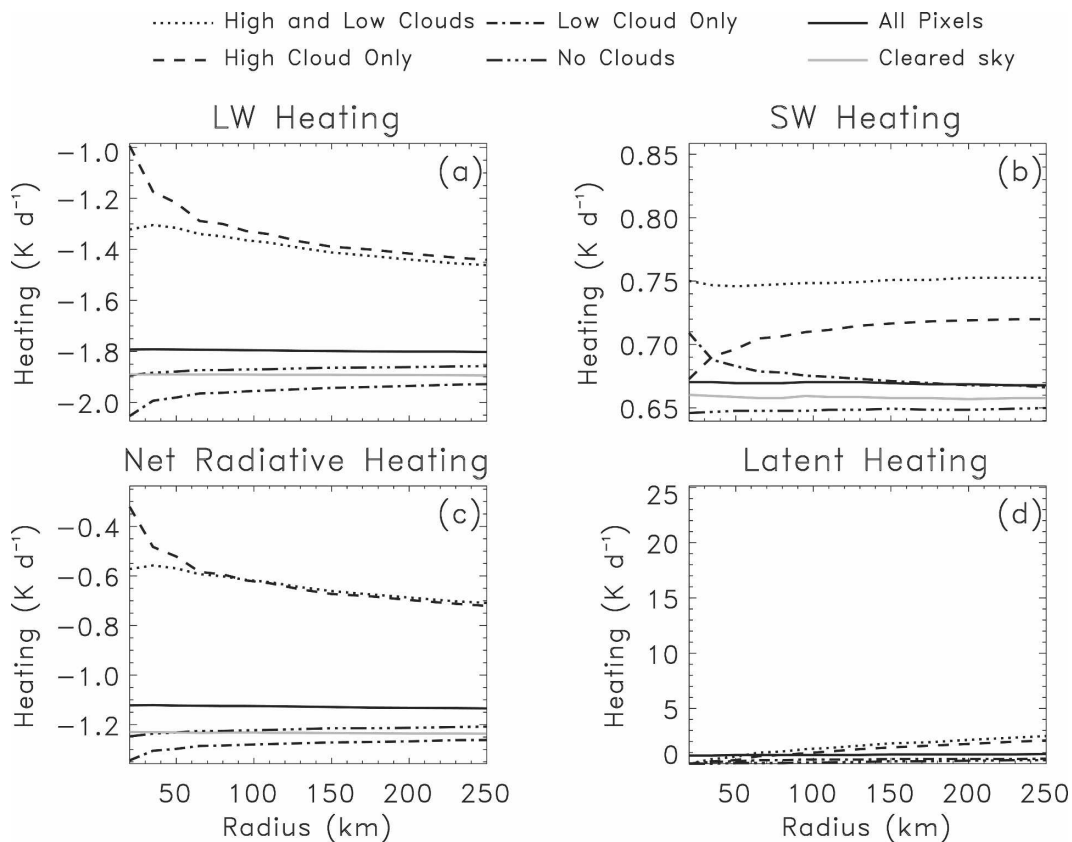
FIG. 5. Same as in Fig. 4, but for nonprecipitating cloud systems.

or-less neutral impact on total column radiative cooling. The impact of the clouds associated with each of the other three precipitation categories on atmospheric SW heating is substantially less than their LW impacts, but all precipitating pixels give rise to a small increase in the absorption of solar radiation. The magnitude of this effect increases with increasing cloud height and decreases monotonically with radial distance from storm center. The LW heating from the two deep categories also decreases with increasing radius resulting from the fact that the optical depth of the cirrus anvil associated with deep convection decays with increasing distance from the precipitation core coupled with the fact that all other precipitation and cloud types exhibit significantly more cooling than the deepest events.

Figure 5 presents analogous results for nonprecipitating pixels separated according to whether they contain both high and low clouds, either type of cloud independently, or no clouds at all. The range of atmospheric SW absorption in nonprecipitating pixels is less than 0.1 K day^{-2} bounded by clear-sky pixels at 0.65 and those containing both high and low clouds at 0.75 K day^{-1}. Differences in column-integrated radiative cooling between the cloud types is, therefore, dominated by

their influence on LW emission to the surface and to space. High-cloud pixels trap the greatest amount of LW radiation and their influence falls off with increasing radius in a manner similar to the deep convective and deep stratiform classes for the reasons noted above. The cloud-free scenes cool at a nearly uniform rate of ~1.8 K day^{-1}, exhibiting only a slight warming with increasing radius, which indicates that the clear areas are generally the largest in spatial extent. Low clouds exhibit the strongest atmospheric LW cooling by virtue of their warm tops and enhanced emission to the surface.

When combined with SW heating, the net atmospheric radiative cooling of the nonprecipitating cloud types spans a range very similar to that of the precipitating systems varying by a factor of 4 between the high-cloud-only and low-cloud-only categories. There is, of course, no latent heating in the immediate area of the nonprecipitating pixels. As the averaging radius is increased, however, some latent heating becomes evident particularly in the areas surrounding high clouds, indicating that they are often associated with precipitating cores, as one might expect.

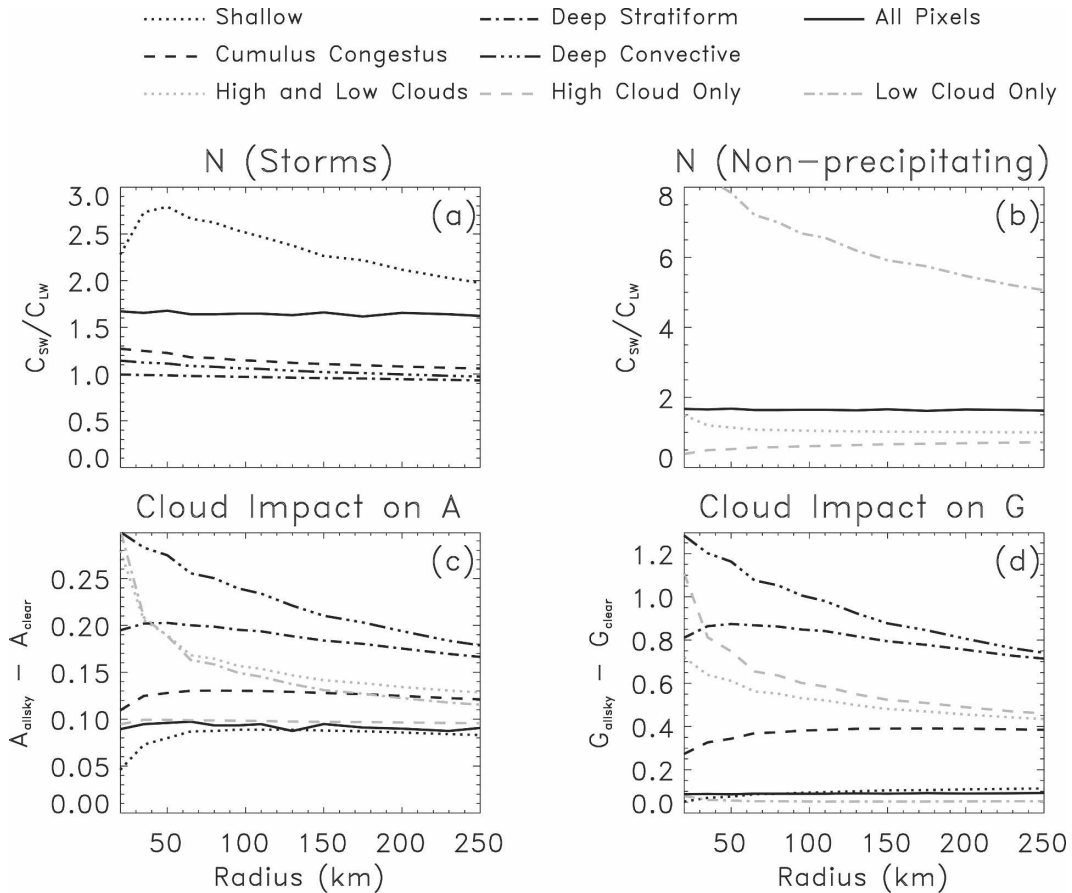In addition to atmospheric heating, there are a vari-

FIG. 6. Mean radiative impacts of each cloud category as a function of radial distance from the central pixel. (a), (b) The ratio of the cloud impact on TOA LW radiation to that on TOA LW radiation for precipitating and nonprecipitating cloud systems, respectively. (c), (d) Cloud impacts on broadband albedo and greenhouse parameter (see text), respectively.

ety of other measures of the impact of clouds on their environment. CESS01, for example, analyze the ratio of cloud impacts on TOA SW to LW fluxes, N, which has the benefit that values greater than (less than) unity are indicative of a net cooling (heating) effect in the atmosphere. This ratio is presented for each storm and cloud type in the upper panels of Fig. 6, respectively. Clearly N is a strong function of the type of cloud being observed. Shallower cloud systems such as the low-cloud and shallow-precipitation category exhibit substantially more SW cooling than LW heating by virtue of their low cloud tops. Deep systems, on the other hand, trap an amount of LW radiation that is approximately equal to the SW radiation they reflect. As a result, N is remarkably close to unity for the deep convective and deep stratiform storm categories and actually less than one for the less reflective nonprecipitating high-cloud category. It is interesting to note that for all other categories cloud SW radiative effects are of the same magnitude or larger than their LW counterparts. When

coupled with the fact that the cloud impact on atmospheric SW heating is generally small (Figs. 4 and 5), this demonstrates that cloud SW cooling is generally felt at the surface rather than in the atmosphere, while the converse holds for LW heating.

Two other useful diagnostics of cloud impacts are provided by their impact on the albedo, $C_A = A_{\text{allsky}} - A_{\text{clear}}$, and the greenhouse parameter defined as the ratio of the flux emitted from the earth's surface to that emitted to space,

$$G = \frac{\sigma T_s^4}{\sigma T_a^4}, \qquad (3)$$

where T_s is the surface temperature and T_a is the equivalent blackbody temperature of the atmosphere (Stephens and Greenwald 1991a,b). The radial variability in these parameters for each storm and cloud type are presented in the lower panels of Fig. 6. Since C_A and $C_G = G_{\text{allsky}} - G_{\text{clear}}$ represent the deviation from

clear-sky conditions, these parameters provide a measure of the magnitude of the cloud impact on SW and LW fluxes while the upper panels compared their relative strengths. The deepest cloud systems are clearly the brightest and exert the strongest influence on the atmospheric greenhouse effect resulting from the fact that they reside at very cold temperatures above a majority of the atmospheric water vapor. The impacts of other cloud systems decrease monotonically with cloud top height consistent with the increasing strength of water vapor absorption and emission with increasing depth in the atmosphere. As a result, low clouds and shallow precipitation exert a factor of 2 smaller impact on albedo than the deep systems and have a minimal effect on the LW greenhouse effect.

This result has important consequences for the magnitude of net heating/cooling averaged over a particular region and time period. The mean ratio of cloud impacts, $\overline{N}$, will, of course, derive from the collective effects of all clouds found within that region. It is important to realize, however, that the impact of any given cloud type on $\overline{N}$ is weighted by the magnitude of its impact on SW and LW fluxes at TOA. As a result, deep convective and high-cloud systems will always dominate $\overline{N}$ in a region where they occur with any regularity by virtue of the fact that they are typically the brightest and coldest clouds. Thus the near cancellation of LW and SW cloud radiative effects in the Tropics observed by Kiehl (1994) is a direct result of the high frequency of occurrence of high-/deep-cloud systems that generally reside in the region, but it does not necessarily preclude the existence of low and midlevel clouds that can play an important role in determining the distribution of lower-tropospheric moisture within the region.

b. Implications for regional energy budgets

The mean energetic properties of each individual precipitating and nonprecipitating cloud category considered in this study are summarized in Fig. 7 with associated error bars that once again represent an upper bound on the uncertainties in heating and cooling estimates. By far the largest source of variability in the heating effects of each category arises from the latent heat release. On average pixels falling into the deep convective category release 3 times as much latent heat in the atmosphere than any other type. Furthermore, as a result of their latent heat release, all precipitating pixels heat the atmosphere while all nonprecipitating pixels cool it.

Given the substantial differences in the radiative and latent heating properties of the different precipitating and nonprecipitating cloud systems, it is easy to see how variability in their relative frequency of occurrence
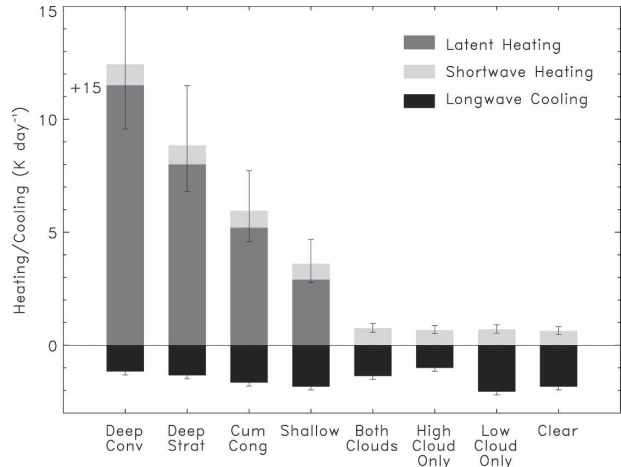

FIG. 7. Mean LW radiative cooling, SW radiative heating, and latent heating properties of each of the storm and cloud types analyzed. Note that the latent heating due to deep convective pixels has been reduced by 15 K day^{-1} to facilitate plotting.

(RFO) can significantly impact the energetic properties of a region. This is demonstrated in Fig. 8 where the mean heating properties of each storm category is weighted by their frequency of occurrence in the TWP in February 1998. Figure 9 provides similar information for February 2000. By breaking the energy budget down in this way, the connection between the reduced atmospheric heating observed during the 1998 El Niño and the reduction in deep convective and stratiform pixels becomes readily apparent. As noted in Part I, there is a distinct reduction in the amount of deep con-
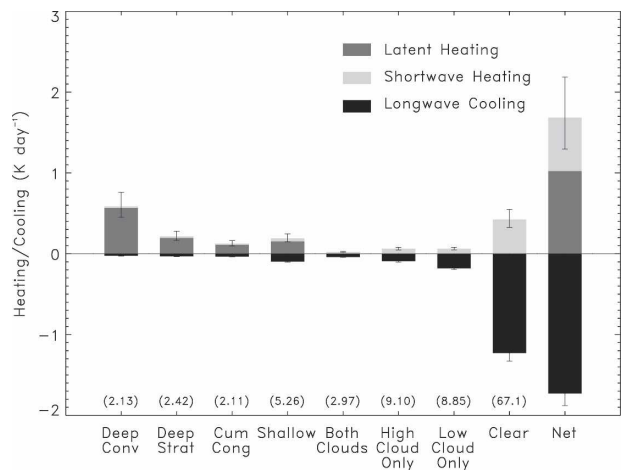

FIG. 8. Net radiative heating/cooling and latent heating in the west Pacific during February 1998 broken down by storm and cloud type. The numbers in parentheses represent the total fraction of pixels that fall into each category and the heating bars on the far right represent the cumulative heating due to all types.
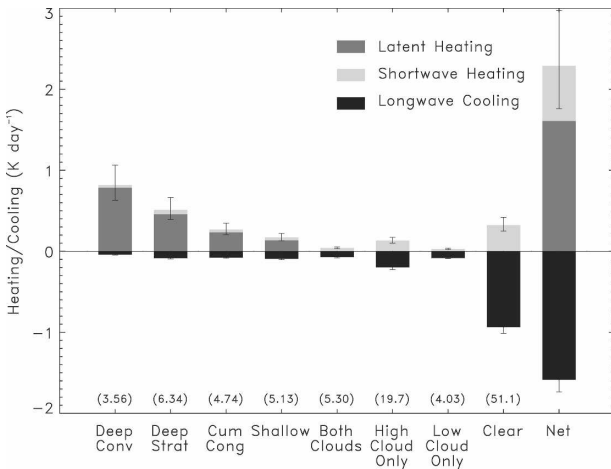
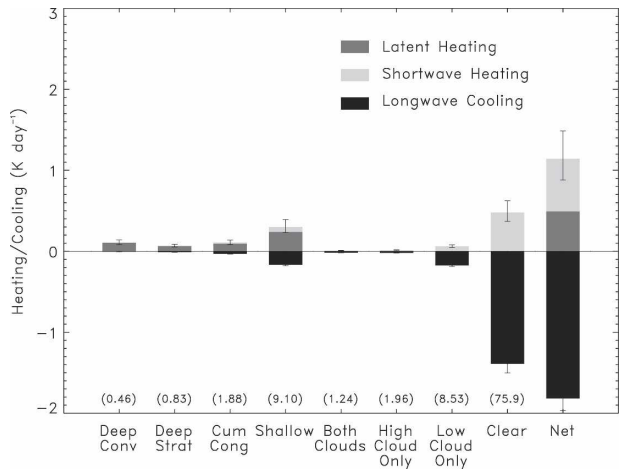FIG. 9. Same as in Fig. 8, but for the month of February 2000.

FIG. 11. Same as in Fig. 10, but for the month of February 2000.

vective and stratiform rainfall and high clouds in February 1998 dramatically reducing the latent heat release in the atmosphere. Simultaneously, the number of cloud-free pixels increases from 51%–67%, substantially increasing the LW radiative cooling in the region. The net result is that the west Pacific goes from being characterized by the generation of intense atmospheric heating implying substantial energy transport out of the region in normal years to exhibiting conditions that approach local RCE during the 1998 El Niño event.

The breakdown of the energy budget in the TEP in February 1998 and 2000 is presented in Figs. 10 and 11, showing precisely the opposite trend. During normal years, rainfall in the region is dominated by shallow precipitation systems while a majority of nonprecipitating systems contains low clouds or is cloud free. This results in LW radiative cooling that exceeds SW and
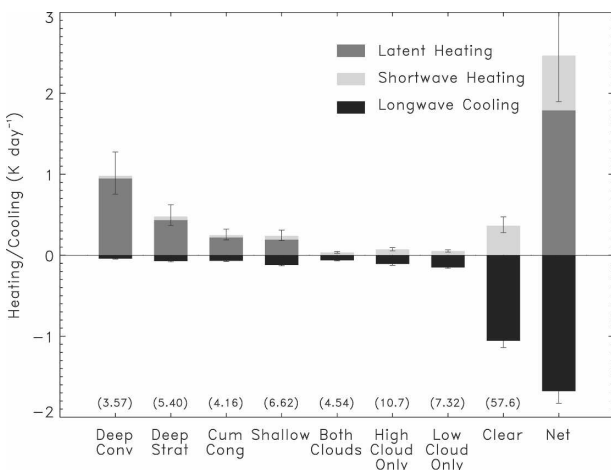
latent heating by more than 50%. The eastward propagation of warm SSTs associated with the 1998 El Niño, however, creates conditions more favorable to the generation of deep convection, resulting in surplus heating in the region. Thus the variations in the distribution of clouds and precipitation that are driven by changes in the SST gradient across the Pacific, shift the ratio of radiative cooling to latent heating in the atmosphere toward local equilibrium in both the east and west Pacific, eliminating the required energy transport to reestablish balance. In normal years, heating preferentially occurs in the west Pacific while cooling occurs in the east, resulting in strong eastward energy transport by the Walker circulation.

It is worth noting that the region of the TWP analyzed in CESS01 (not shown) exhibits the same general features as those in Figs. 8 and 9. This suggests that the observed change in the net influence of clouds on TOA radiative fluxes that occurred during the 1998 El Niño are tied to a fundamental shift in the character of precipitation systems from the deep convective events typical of normal years to less intense midlevel and shallow systems that reflect more solar radiation than trap LW radiation. Interestingly, in both February 1998 and 2000, 13% of the pixels in the TWP fall into the low and midlevel precipitation and cloud categories. The fraction of deep systems in these regions, however, decreases from 36% in the normal year to 14% during the 1998 El Niño. This indicates that the deviation of the cloud effect ratio from 1.0 noted in CESS01 is a direct consequence of the reduction of high-/deep-cloud systems that ordinarily dominate the net radiative effects of clouds in the region. The results further indicate that this shift in cloud type does more than just modify TOA radiative fluxes—it completely changes the character of

FIG. 10. Same as in Fig. 8, but for the east Pacific.

TABLE 6. Linear cloud surface cooling and atmospheric heating efficiencies (Bretherton and Sobel 2002) and their relationship to local environmental parameters in the three study regions during February 1998 and 2000. HCF and PF are expressed in percent and are mutually exclusive (i.e., both cloud categories include only nonprecipitating pixels).

Year	Region	SST (K)	W (kg m^{-2})	V_{av} (m s^{-1})	HCF	PF	r_C	r_H
1998	TWP	301.8	47.8	5.91	16.62	11.92	0.206	0.160
2000	TWP	302.4	53.4	3.75	34.90	19.77	0.176	0.168
1998	TCP	301.7	50.4	7.76	32.36	17.72	0.164	0.152
2000	TCP	299.6	36.8	6.21	4.90	8.93	0.259	0.035
1998	TEP	301.9	50.4	5.78	24.21	19.75	0.145	0.125
2000	TEP	298.9	41.6	3.91	4.49	12.27	0.305	0.047

the TWP from a source of atmospheric heating to a region in which an approximate balance between the radiative cooling and latent heat released in precipitation result in a local thermal equilibrium that temporarily isolates it (energetically) from the rest of the Tropics.

5. Discussion

The results from Part I and the previous sections offer quantitative evidence that the distribution and character of precipitating cloud systems found in the tropical Pacific exhibit significant responses to the SST anomalies associated with El Niño. The resulting changes in clouds and precipitation in turn influence the thermal and hydrologic properties of each region as evidenced by the changes in latent and cloud radiative heating of the atmosphere, solar heating at the surface, and transport of water vapor to upper levels by the implied convective air motions associated with the observed deep systems. Together these observations imply the existence of strong feedbacks owing to the interdependencies of SST, water vapor, clouds, precipitation, and radiation that must be modeled in order to accurately represent the coupled response of these quantities in a climate change scenario. In this section, we explore some additional diagnostics that may provide insights into the strengths of these feedbacks and examine their relationship to their environment.

Table 6 summarizes a number of properties of the three analysis regions in February 1998 and 2000. The signature of El Niño is clearly evident in the dramatic warming of SSTs in the TEP and TCP during February of 1998. Also evident are increases in both W and mean surface wind speed during this period indicative of the increased evaporation from the surface due to the warmer SSTs and the stronger winds found in the inflow and outflow regions associated with deep convection. There is also evidence of increased amounts of high cloud associated with precipitation over warmer SSTs. This is most notable for the TCP and TEP where

the ratio of high cloud area to precipitation area is considerably less than one during the normal year but exceeds unity above the warmer SSTs associated with the 1998 El Niño. While less dramatic, a similar trend can be seen in the TWP where the ratio of high cloud fraction (HCF) to precipitating cloud fraction (PF) decreases during the El Niño year. These results demonstrate that changes in the Walker circulation in response to El Niño lead to more extensive areas of high clouds for a given precipitation area in regions of warmer SST. This is not to say that the precipitation efficiency decreases with increasing SST, however, since the comparison relates cloud area to precipitation area rather than rainfall intensity. In fact, the results of Rapp et al. (2005) suggest that the ratio of high-cloud area to surface rain amount is invariant to changes in SST for all but the warmest clouds, which show a decrease with increasing SST.

In light of feedback studies like that of Lindzen et al. (2001), there is considerable value in examining quantities related to precipitation efficiency. Rather than repeating the analysis of Rapp et al. (2005), however, we examine two parameters that relate the radiative impact clouds to surface rainfall in the last two columns of Table 6. These quantities are analogous to the cloud feedback parameter adopted by Bretherton and Sobel (2002) to represent cloud radiative feedbacks in their model of the Walker circulation. Motivated by the need to provide their model with a simple, yet plausible, representation of the impact of precipitation on radiative flux divergence in the atmosphere, they assume that clouds reduce the clear-sky radiative cooling by an amount proportional to precipitation, P, via

$$R = R_0 - rP, \tag{4}$$

where R_0 represents cooling in the absence of clouds. Bretherton and Sobel (2002) assume a value of $r = 0.2$ and note that its uncertainties may be as large as 50% because of constraints imposed the datasets used to define it. Sobel and Gildor (2003) adopt a similar parameterization in their coupled ocean–atmosphere model

used to explore the role of clouds in modulating SST hot spots. They further assume that cloud-induced SW cooling of the ocean surface is governed by an identical relationship, $S = \hat{S} - rP$, noting the approximate cancellation in SW and LW cloud radiative effects at TOA in regions dominated by high clouds as justification.

While these simple relationships were born from practical modeling considerations, the linear radiative feedback parameter, r, provides a useful measure of the extent to which precipitating systems radiatively heat the atmosphere and cool the surface that also varies in response to El Niño. However, since we are not motivated by the need for simplicity, we define distinct values of r corresponding to both the cloud SW cooling effect at the surface,

$$r_C = -1.0 \times \frac{(F^{\downarrow}_{\text{SW,SFC}})_{\text{allsky}} - (F^{\downarrow}_{\text{SW,SFC}})_{\text{clrsky}}}{\text{LH}}, \quad (5)$$

and the radiative heating in the atmosphere,

$$r_H = \frac{(\Delta F_{\text{LW}} + \Delta F_{\text{SW}})_{\text{allsky}} - (\Delta F_{\text{LW}} + \Delta F_{\text{SW}})_{\text{clrsky}}}{\text{LH}},$$

$$(6)$$

where $\Delta F_{\text{LW}} = F^{\uparrow}_{\text{LW,SFC}} - F^{\downarrow}_{\text{LW,SFC}} - F^{\uparrow}_{\text{LW,TOA}}$ and $\Delta F_{\text{SW}} = F^{\downarrow}_{\text{SW,TOA}} + F^{\uparrow}_{\text{SW,SFC}} - F^{\downarrow}_{\text{SW,SFC}} - F^{\uparrow}_{\text{SW,TOA}}$ are the LW and SW atmospheric flux divergence, respectively, while LH denotes the latent heating equivalent of surface precipitation. Here, r_H and r_C can be viewed as measuring the efficiency with which a storm system radiatively heats the atmosphere and cools the surface per unit rainfall rate or, equivalently, latent heat release in the atmosphere. Since the net radiative impact of a cloud system depends, in part, on its spatial extent and total mass, these quantities are closely related to the more traditional precipitation efficiency defined as the ratio of precipitation to total condensate. They may, however, provide a closer link to the true physical processes by which clouds feed back on their environment since they represent a direct measure of a storm's role in establishing the local gradients in atmospheric heating that ultimately drive changes in stability.

Unlike the model of Sobel and Gildor (2003), where r_C and r_H are assumed equal and held fixed independent of the changing SST in their column model, Table 6 shows that the heating and cooling efficiencies of precipitating systems vary significantly between El Niño and normal conditions. Furthermore, the efficiency of a storm system to cool the surface and its ability to warm the atmosphere seem to respond to ENSO in opposite ways. In the TEP, for example, r_H increases with the onset of El Niño resulting from a shift toward deeper, colder cloud systems with larger high-cloud anvils,

while r_C decreases possibly because of an increase in the precipitation efficiency of shallow, warm rain systems consistent with the findings of Lau and Wu (2003) and Rapp et al. (2005). As a result, storms in the TCP and TEP cool the surface much more efficiently than they heat the atmosphere under normal conditions, while r_C and r_H are nearly equal over the much warmer SSTs during the 1998 El Niño event. In the TWP, both efficiencies are equal with a value of ~0.17 under normal conditions but the slight cooling in the TWP leads to a shift toward greater surface cooling than atmosphere heating during the El Niño.

It is interesting to note that these trends in r_H and r_C manifest themselves on time and space scales other than that of the El Niño. Figures 12a and 12c present scatterplots of 20-day mean values of r_H and r_C, respectively, as functions of SST for 10° pixels in the TEP. While there is significant variability from pixel to pixel, r_C exhibits a distinct decrease with increasing SST in the statistical sense. Conversely, r_H generally increases with SST, particularly over cooler waters approaching a constant value for SST > 301.5. These results suggest that in the TEP both the ability of a precipitating cloud system to heat the atmosphere and cool the surface vary with SST in a systematic way. It is important to note, however, that the satellite observations themselves cannot establish the mechanism governing the observed dependences of r_C and r_H on SST. The analyses of Fu et al. (1990), Lau et al. (1997), and Bony et al. (1997), for example, suggest that the observed changes in radiative efficiency are likely manifestations of variations in large-scale ascent that may occur in response to changes in local SST gradients. In fact, Figs. 12b and 12d demonstrate that trends in the TWP are substantially smaller than those in the TEP, suggesting that factors other than SST govern variations in r_C and especially r_H at SSTs warmer than 302 K; this is consistent with the findings of Bony et al. (1997), who demonstrate that large-scale vertical motion is largely decoupled from SST above 302.5 K in reanalysis datasets. The explicit representation of precipitation intensity in the radiative efficiencies now allow us to conclude that the changes in OLR and shortwave cloud forcing with SST reported by Bony et al. (1997) and Lau et al. (1997), respectively, are indeed traced to systematic changes in precipitation efficiency. Thus with the exception of regions with the warmest waters, SST provides a useful proxy for the physical processes that govern the ability of a storm system to radiatively heat the atmosphere and cool the surface. The impact of these dependencies on the local radiation balance of the TEP and TWP during an El Niño event is clearly evident from the preceding analysis, but further investigation is
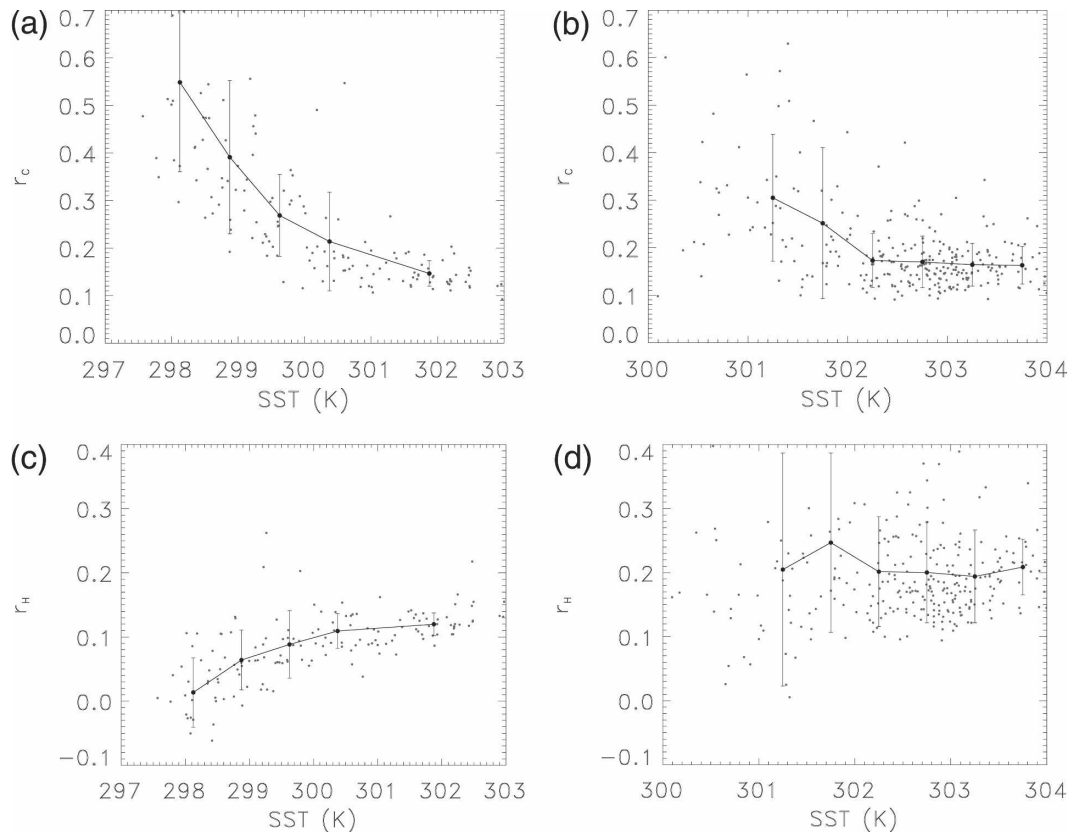
FIG. 12. SST vs r_C: (a) in the TEP and (b) in the TWP. (c), (d) Equivalent results for SST vs r_H for each region. Each data point represents a 20-day average at a resolution of $10° \times 10°$. The solid lines and error bars represent the mean and standard deviation of each parameter in the indicated SST bin.

required to assess their implications for cloud–radiation feedbacks on global scales.

The sensitivity of cloud radiative efficiencies to the properties they act to modify introduces a new level of complexity in modeling cloud feedbacks. Numerous competing processes are at work that collectively determine the regional responses to the forcing that has been introduced. Some of these processes reinforce one another, like the excess latent heat release in the east and central Pacific, the weakening of the Walker circulation, and even the role of wind-induced enhanced evaporation from the ocean's surface that may play a role in maintaining available moisture to sustain convection in these regions. On the other hand, cloud radiative heating at upper levels coupled with SW cooling at the surface has a stabilizing effect on the environment, while decreased cloudiness in the TWP allows more solar radiation to reach the surface acting to reestablish the temperature gradients that are present under normal conditions. The challenge of correctly representing the relative magnitudes of all of these effects puts an enormous burden on model physics. Through

satellite-based studies of the combined response of atmospheric energetics and hydrology, however, constraints can be levied against model parameterizations that should ultimately drive them toward the best possible representation of the climate system.

It is important to note that feedback processes themselves have not been studied in this paper. To do so requires an in-depth analysis of the evolution of precipitation systems in the region and detailed study of the particular interactions between their constituent elements. Instead, the results presented here are intended to demonstrate the complexity of the relationships that underlie the response of regional energy budgets to large-scale forcings like SST variability associated with ENSO. In addition, they highlight the benefits of combining multisensor satellite observations to gain a deeper understanding of critical feedback processes in the climate system. As our ability to represent the physical processes that govern the generation of clouds and precipitation advances, numerical models should become capable of capturing regional and temporal variability in the magnitudes of cloud radiative

effects at TOA and the surface, their ratio, and the atmospheric heating and surface cooling efficiencies described above. This study and its companion paper demonstrate that progress toward this goal requires that models be able to explicitly represent the distributions of distinct precipitating and nonprecipitating cloud types and account for their evolution in response to climate forcings like ENSO. Further study of datasets like these will ultimately allow us to isolate dominant feedback mechanisms and establish their impact on the environment so that parameterizations may be developed to test and eventually constrain parameterizations of cloud radiative effects in climate models.

REFERENCES

Arking, A., 1991: The radiative effects of clouds and their impact on climate. *Bull. Amer. Meteor. Soc.,* **72,** 795–813.

Bony, S., K.-M. Lau, and Y. C. Sud, 1997: Sea surface temperature and large-scale circulation influences on tropical greenhouse effect and cloud radiative forcing. *J. Climate,* **10,** 2055–2077.

Bretherton, C. S., and A. H. Sobel, 2002: A simple model of a convectively coupled Walker circulation using the weak temperature gradient approximation. *J. Climate,* **15,** 2907–2920.

Cess, R. D., M. Zhang, B. A. Wielicki, D. F. Young, X.-L. Zhou, and Y. Nikitenko, 2001: The influence of the 1998 El Niño upon cloud-radiative forcing over the Pacific parm pool. *J. Climate,* **14,** 2129–2137.

Chambers, L. H., B. Lin, and D. F. Young, 2002: Examination of new CERES data for evidence of tropical Iris feedback. *J. Climate,* **15,** 3719–3726.

Cooper, S. J., T. S. L'Ecuyer, and G. L. Stephens, 2003: The impact of explicit cloud boundary information on ice cloud microphysical property retrievals from infrared radiances. *J. Geophys. Res.,* **108,** 4107, doi:10.1029/2002JD002611.

Cornejo-Garrido, A. G., and P. H. Stone, 1977: On the heat balance of the Walker circulation. *J. Atmos. Sci.,* **34,** 1155–1162.

Del Genio, A. D., and W. Kovari, 2002: Climatic properties of tropical precipitating convection under varying environmental conditions. *J. Climate,* **15,** 2597–2615.

Fu, R., A. D. Del Genio, and W. B. Rossow, 1990: Behavior of deep convective clouds in the tropical Pacific deduced from ISCCP radiances. *J. Climate,* **3,** 1129–1152.

Gray, W. M., 1973: Cumulus convection and larger scale circulations. I. Broadscale and mesoscale considerations. *Mon. Wea. Rev.,* **101,** 839–855.

Greenwald, T. J., G. L. Stephens, T. H. Vonder Haar, and D. L. Jackson, 1993: A physical retrieval of cloud liquid water over the global oceans using Special Sensor Microwave/Imager (SSM/I) observations. *J. Geophys. Res.,* **98,** 18 471–18 488.

Hartmann, D. L., and D. A. Short, 1980: On the use of earth radiation budget statistics for studies of clouds and climate. *J. Atmos. Sci.,* **37,** 1233–1250.

——, and M. L. Michelsen, 2002: No evidence for Iris. *Bull. Amer. Meteor. Soc.,* **83,** 249–254.

——, H. H. Hendon, and R. A. Houze Jr., 1984: Some implications of the mesoscale circulations in tropical cloud clusters for large-scale dynamics and climate. *J. Atmos. Sci.,* **41,** 113–121.

——, M. E. Ockert-Bell, and M. L. Michelsen, 1992: The effect of cloud type on earth's energy balance: Global analysis. *J. Climate,* **5,** 1281–1304.

Houze, R. A., Jr., 1982: Cloud clusters and large-scale vertical motions in the tropics. *J. Meteor. Soc. Japan,* **60,** 396–409.

——, 1989: Observed structure of mesoscale convective systems and implications for large-scale heating. *Quart. J. Roy. Meteor. Soc.,* **115,** 425–461.

Jakob, C., 2002: Ice clouds in Numerical Weather Prediction Models—Progress, problems, and prospects. *Cirrus,* D. K. Lynch et al., Eds., Oxford University Press, 327–345.

Kiehl, J. T., 1994: On the observed near cancellation between longwave and shortwave cloud forcing in tropical regions. *J. Climate,* **7,** 559–565.

Kummerow, C. D., and Coauthors, 2000: The status of the Tropical Rainfall Measuring Mission (TRMM) after two years in orbit. *J. Appl. Meteor.,* **39,** 1965–1982.

Lau, K.-M., and L. Peng, 1987: Origin of low-frequency (intraseasonal) oscillations in the tropical atmosphere. Part I: Basic theory. *J. Atmos. Sci.,* **44,** 950–972.

——, and H.-T. Wu, 2003: Warm rain processes over tropical oceans and climate implications. *Geophys. Res. Lett.,* **30,** 2290, doi:10.1029/2003GL018567.

——, ——, and S. Bony, 1997: The role of large-scale atmospheric circulation in the relationship between tropical convection and sea surface temperature. *J. Climate,* **10,** 381–392.

L'Ecuyer, T. S., and G. L. Stephens, 2003: The tropical oceanic energy budget from the TRMM perspective. Part I: Algorithm and uncertainties. *J. Climate,* **16,** 1967–1985.

Lee, M.-I., I.-S. Kang, J.-K. Kim, and B. E. Mapes, 2001: Influence of cloud-radiation interaction on simulating tropical intraseasonal oscillation with an atmospheric general circulation model. *J. Geophys. Res.,* **106,** 14 219–14 233.

Lin, B., B. A. Wielicki, L. H. Chambers, Y. Hu, and K.-M. Xu, 2002: The iris hypothesis: A negative or positive cloud feedback? *J. Climate,* **15,** 3–7.

Lindzen, R. S., M. D. Chou, and A. Hou, 2001: Does the earth have an adaptive infrared iris? *Bull. Amer. Meteor. Soc.,* **82,** 417–432.

Mapes, B. E., and R. A. Houze Jr., 1995: Diabatic divergence profiles in western Pacific mesoscale systems. *J. Atmos. Sci.,* **52,** 1807–1828.

Masunaga, H., T. S. L'Ecuyer, and C. Kummerow, 2005: Variability in the characteristics of tropical precipitation systems. Part I: Spatial structure. *J. Climate,* **18,** 823–840.

Pierrehumbert, R. T., 1995: Thermostats, radiator fins, and the local runaway greenhouse. *J. Atmos. Sci.,* **52,** 1784–1806.

Ramanathan, V., and W. Collins, 1991: Thermodynamic regulation of ocean warming by cirrus clouds deduced from observations of the 1987 El Niño. *Nature,* **351,** 27–32.

Rapp, A. D., C. Kummerow, W. Berg, and B. Griffith, 2005: An evaluation of the proposed mechanism of the adaptive infrared iris hypothesis using TRMM VIRS and PR measurements. *J. Climate,* **18,** 4185–4194.

Sherwood, S. C., V. Ramanathan, T. P. Barnett, M. K. Tyree, and E. Roeckner, 1994: Response of an atmospheric general circulation model to radiative forcing of tropical clouds. *J. Geophys. Res.,* **99,** 20 829–20 845.

Slingo, A., and J. M. Slingo, 1988: The response of a general circulation model to cloud longwave radiative forcing. I: Introduction and initial experiments. *Quart. J. Roy. Meteor. Soc.,* **114,** 1027–1062.

Slingo, J. M., and A. Slingo, 1991: The response of a general circulation model to cloud longwave radiative forcing. II: Further studies. *Quart. J. Roy. Meteor. Soc.,* **117,** 333–364.

Sobel, A. H., and H. Gildor, 2003: A simple time-dependent model of SST hot spots. *J. Climate,* **16,** 3978–3992.

Stephens, G. L., 2005: Cloud feedbacks in the climate system: A critical review. *J. Climate,* **18,** 237–273.

——, and T. J. Greenwald, 1991a: The Earth's radiation budget and its relation to atmospheric hydrology. 1. Observations of the clear sky greenhouse effect. *J. Geophys. Res.,* **96,** 15 311–15 324.

——, and ——, 1991b: The Earth's radiation budget and its relation to atmospheric hydrology. 2. Observations of cloud effects. *J. Geophys. Res.,* **96,** 15 325–15 340.

——, S.-C. Tsay, J. P. W. Stackhouse, and P. J. Flatau, 1990: The relevance of the microphysical and radiative properties of cirrus clouds to climate and climate feedback. *J. Atmos. Sci.,* **47,** 1742–1753.

——, P. M. Gabriel, and P. T. Partain, 2001: Parameterization of atmospheric radiative transfer. Part I: Validity of simple models. *J. Atmos. Sci.,* **58,** 3391–3409.

Vonder Haar, T. H., and V. E. Suomi, 1971: Measurements of the Earth's radiation budget from satellites during a five-year period. Part I: Extended time and space means. *J. Atmos. Sci.,* **28,** 305–314.

Wielicki, B. A., B. R. Barkstrom, E. F. Harrison, R. B. Lee III, G. L. Smith, and J. E. Cooper, 1996: Clouds and the Earth's Radiant Energy System (CERES): An Earth Observing System experiment. *Bull. Amer. Meteor. Soc.,* **77,** 853–868.